Electronic supporting information

Insertion of single-ion magnets based on mononuclear Co(II) complexes into ferromagnetic oxalate-based networks

M. Palacios-Corella,[a] V. García-López,[a] C. Sánchez-Sánchez,[a,b] J. M. Clemente-Juan,[a] M. Clemente-León[a] and E. Coronado[a]

[a.] *Instituto de Ciencia Molecular (ICMol), Universidad de Valencia, C/ Catedrático José Beltrán 2, 46980 Paterna, Spain. Fax: 34 963543273; Tel: 34 963544419; E-mail: miguel.clemente@uv.es.*
[b.] *Present address.*

ESI 1. Structure of 1

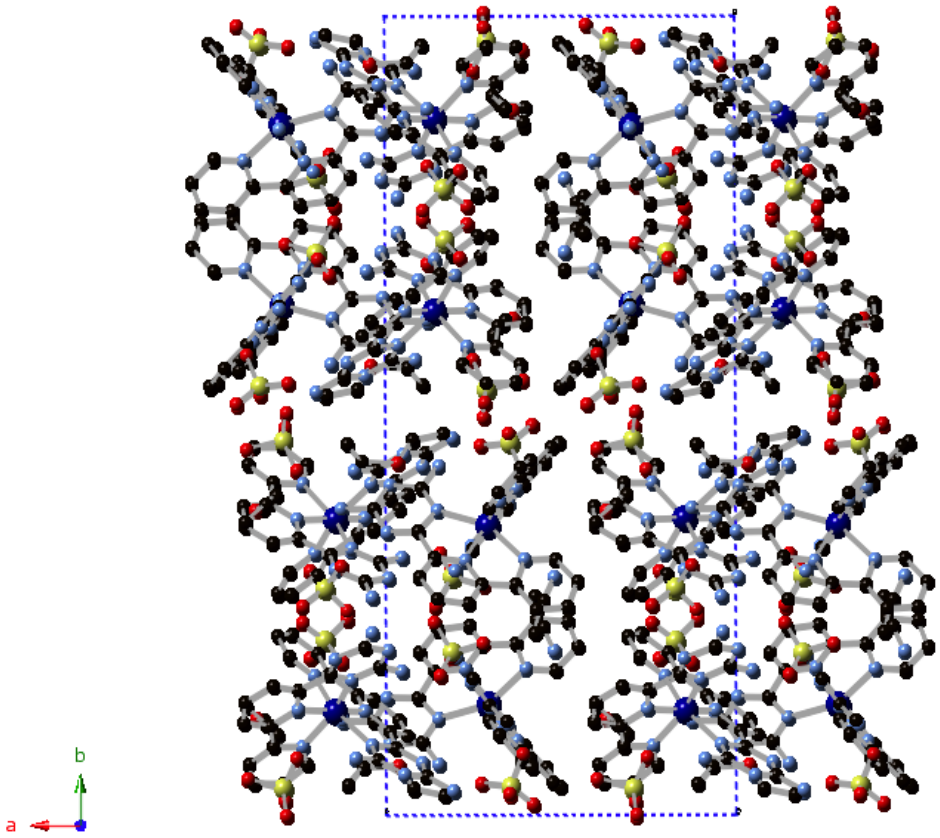

Fig. S1 Projection on the *ab* plane of the structure of **1;** Co (dark blue), Cl (yellow), C (black), N (blue), O (red); hydrogen atoms have been omitted for clarity.

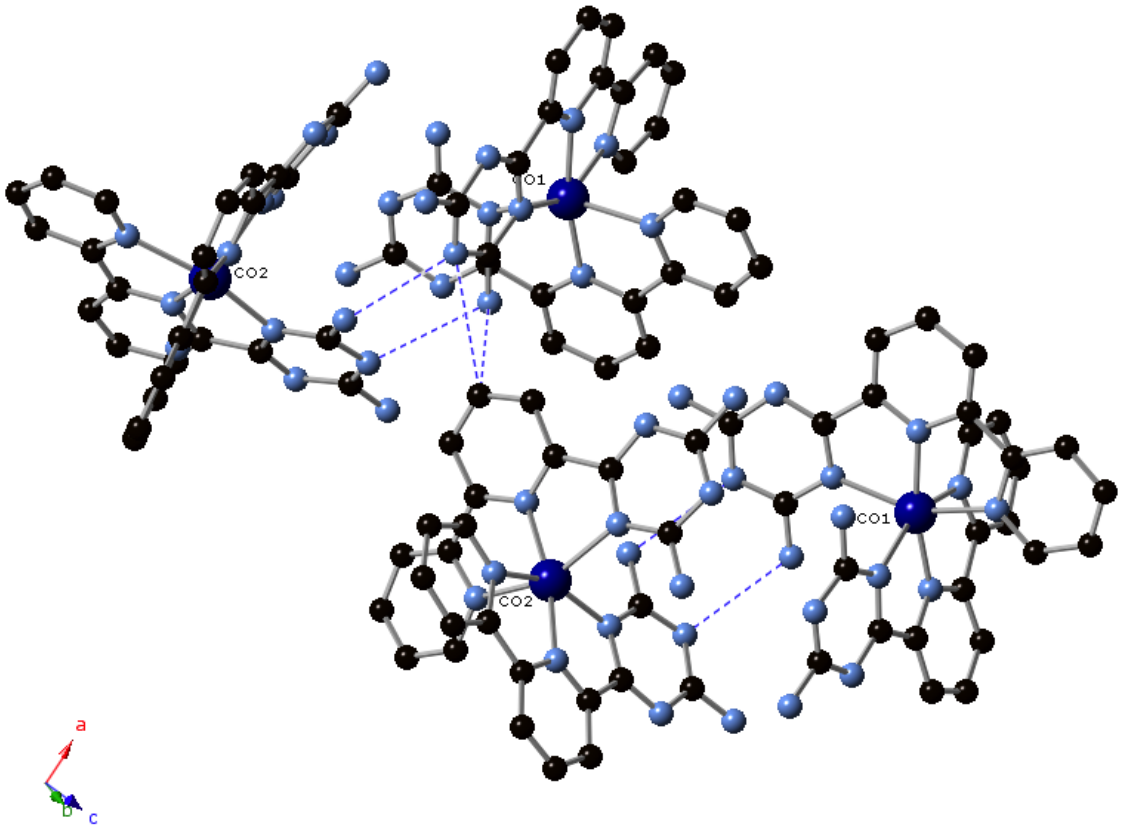

Fig. S2 Two dimers of neighbouring $[Co^{II}(L_1)_2]^{2+}$ linked through CH···N short contacts in **1;** Co (dark blue), C (black), N (blue), O (red); hydrogen atoms have been omitted for clarity.

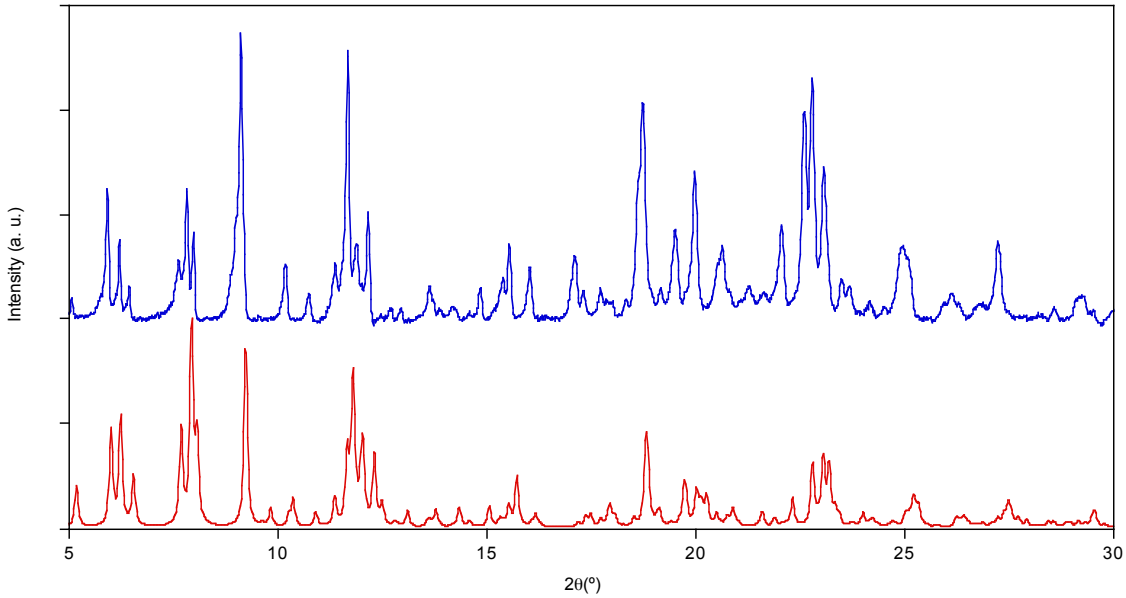

Fig. S3 Powder X-ray diffraction pattern of **1** at room temperature measured in contact with the mother liquor (blue) and simulated one from single crystal X-ray diffraction data at 300 K (red).

ESI 2. Structure of 2

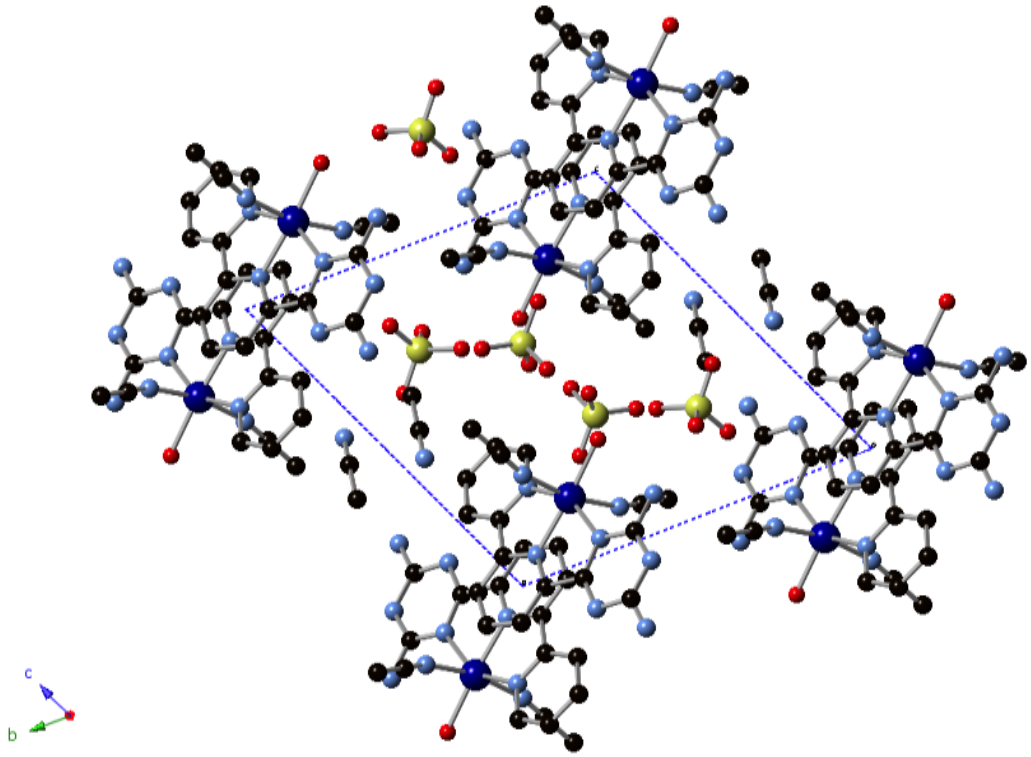

Fig.S4 Projection on the *bc* plane of the structure of **2;** Co (dark blue), Cl (yellow), C (black), N (blue), O (red); hydrogen atoms have been omitted for clarity.

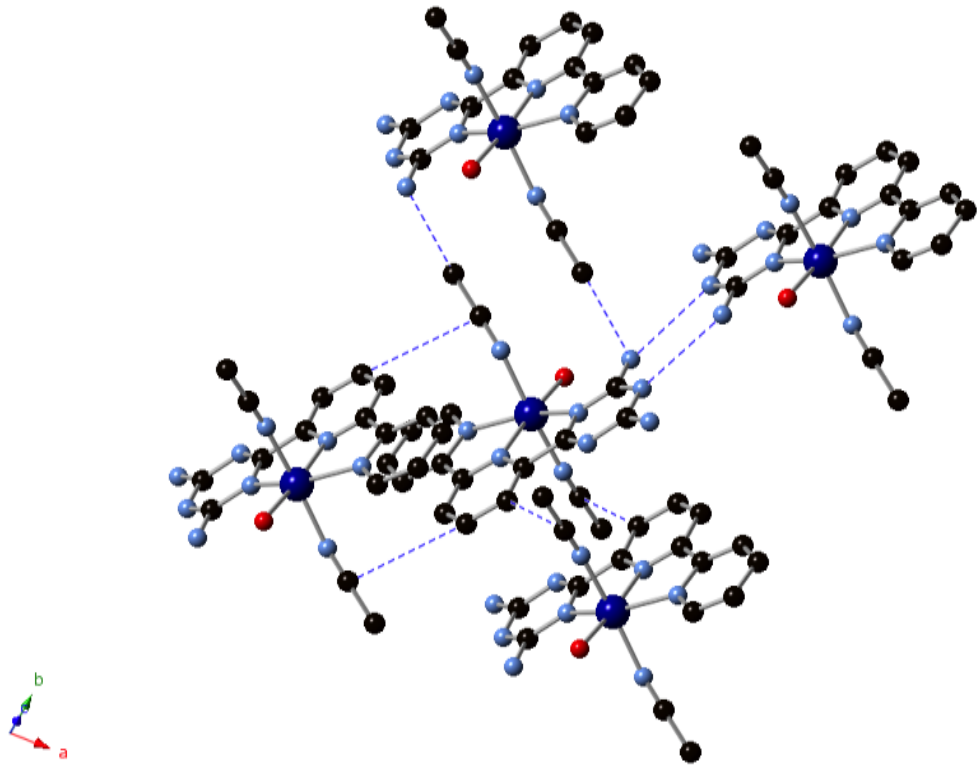

Fig. S5 Short contacts between neighbouring $[Co^{II}(L_1)(CH_3CN)_2(H_2O)]^{2+}$ complexes in the structure of **2;** Co (dark blue), Cl (yellow), C (black), N (blue), O (red); hydrogen atoms have been omitted for clarity.

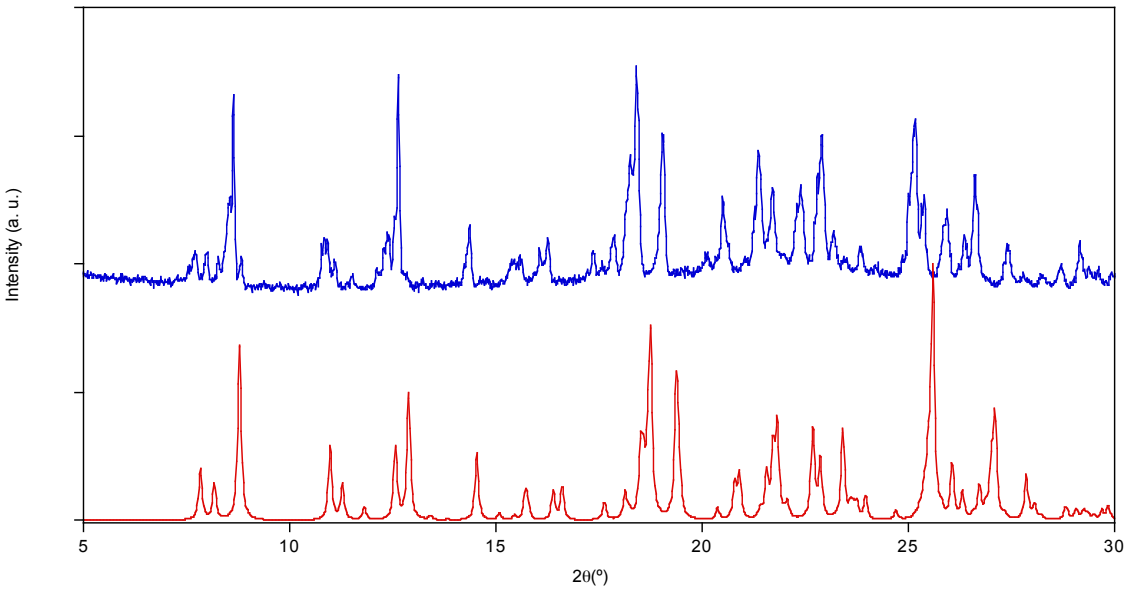

Fig. S6 Powder X-ray diffraction pattern of **2** at room temperature measured in contact with the mother liquor (blue) and simulated one from single crystal X-ray diffraction data at 120 K (red).

ESI 3. Structure of 3

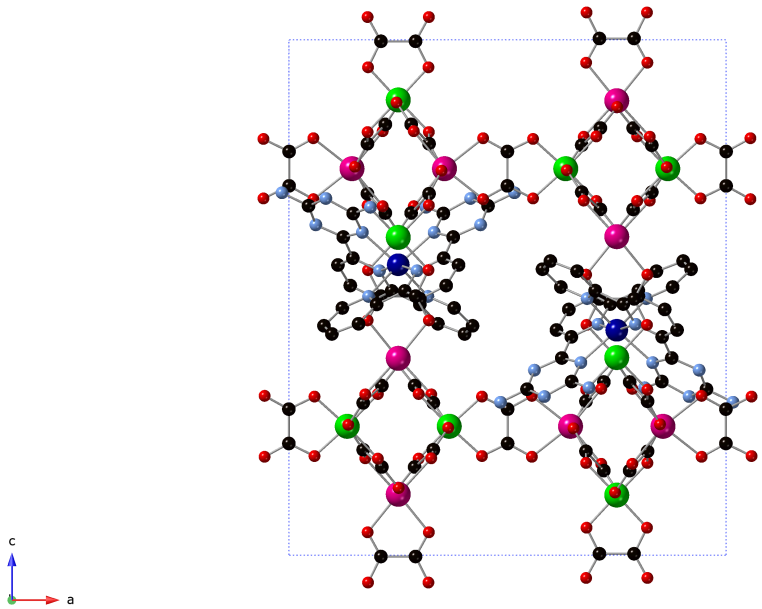

Fig. S7 Projection on the *ac* plane of the structure of **3;** Co (dark blue), C (black), N (blue), O (red), Mn (pink) and Cr (green); hydrogen atoms have been omitted for clarity.

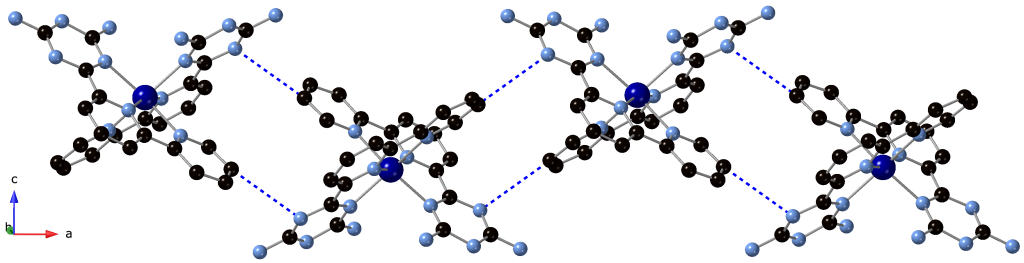

Fig. S8 Chains of $[Co^{II}(L)_2]^{2+}$ complexes running along the *a* axis linked through CH···N intermolecular interactions (blue dashed lines) in the structure of **3;** Co(dark blue), N (blue), C (black).

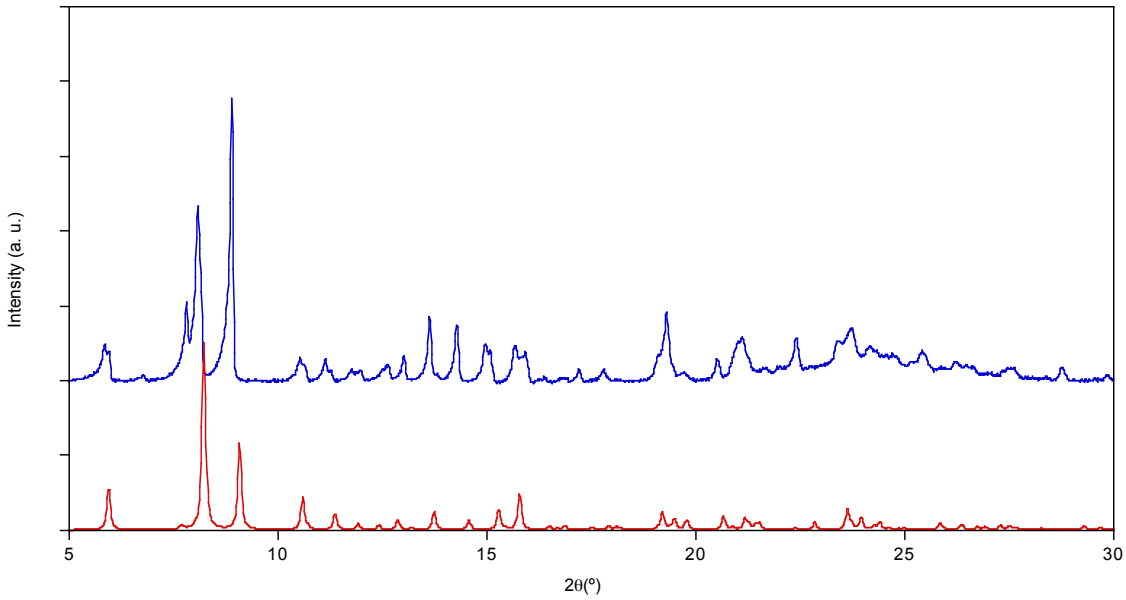

Fig. S9 Powder X-ray diffraction pattern of **3** at room temperature measured in contact with the mother liquor (blue) and simulated one from single crystal X-ray diffraction data at 120 K (red).

ESI 3. Structure of 4

Structure of $[Co^{II}(L)_2][Mn^{II}Cr^{III}(ox)_3]_2\cdot$(solvate) (4). 4 crystallizes in the monoclinic space group $P2_1/n$. It is formed by anionic layers with a distorted 2D bimetallic oxalate network of formula $[Mn^{II}(H_2O)_{0.67}Cr^{III}(ox)_3]^-$ in the *bc* plane alternating with a layer of $[Co^{II}(L_1)_2]^{2+}$ complexes and disordered solvent molecules (see **Fig. S10**). The bimetallic oxalate anionic layer presents the well-known honeycomb structure formed by an extended network of Mn(II) and Cr(III) ions linked through oxalate bridges. These oxalate ligands connect the Mn(II) and Cr(III) ions in such a way that each Mn(II) is surrounded by three neighboring Cr(III) and *vice-versa*. The neighbouring octahedral metal centres of the bimetallic oxalate network present alternated chirality as usual for this type of network. It contains three crystallographically independent Mn(II) ions and Cr(III) ions, which can be distinguished by their typical M-O distances (2.157(8)-2.328(14) Å for Mn and 1.943(9)-2.003(8) Å for Cr). Cr(III) ions exhibit a distorted octahedral coordination as that of one of the three crystallographically independent Mn(II) ions (Mn2). The other two Mn(II) ions (Mn1 and Mn3) are heptacoordinated. Thus, the six O from the three oxalate ligands form a distorted octahedron with Mn–O distances ranging from 2.196(7) to 2.320(9) Å for Mn1 and from 2.198(7) to 2.306(8) Å for Mn3, which is capped with a coordinated water molecule at Mn-O distances of 2.328(14 (Mn1) and 2.196(9) Å (Mn3). The heptahedral coordination of 2/3 of the Mn(II) ions distorts the honeycomb structure in such a way that the Mn(II) ions are out of the plane defined by the Cr(III) ions in contrast to other 2D oxalate structures. This effect is more important for the two heptacoordinated Mn(II) ions (Mn1 and Mn3) that are clearly above and below the plane defined by the Cr(III) ions (**Fig. S10**). The water solvent molecules coordinated to these two Mn(II) sites are perpendicular to the oxalate layers pointing to opposite neighbouring layers. A similar effect has been observed in other compounds reported in the literature containing honeycomb layers with solvent molecules coordinated to Mn(II).[1,2] The minimum distance between metal ions belonging to different oxalate layers is 10.62 Å, which is slightly lower to that found in 2D compounds with $[Fe^{II}(L)_2]^{2+}$ (11.24 Å)[3] and $[Fe^{III}(sal_2\text{-trien})]^+$ and derivatives (11.609-11.644 Å),[4] due to the distortion of the layers.

The space between the oxalate layers is occupied by one and a half crystallographically independent $[Co^{II}(L)_2]^{2+}$ complexes and disordered solvent molecules. The $[Co^{II}(L)_2]^{2+}$ complex with an occupancy 0.5 presents a disorder with two possible configurations. The Co(II) presents a distorted N_6 octahedral coordination to the two tridentate L ligands as tht of **1** and **3**.

The Co-N bond lengths of the inner pyridine and triazine rings are 2.050(11)-2.071(10) Å (Co1) and 2.078(18)-2.08(2) Å (Co2) and 2.138(11)-2.191(11) Å (Co1) and 2.145(9)-2.192(18) Å (Co2), respectively, while those of the external pyridine ring are 2.186(10)-2.211(11) Å (Co1) and 2.094(12)-2.162(11) Å (Co2). These distances are very similar to those of **1** and **3** and typical of Co(II) in the high-spin state. There are several hydrogen-bonds between the NH_2 from triazine group of L and oxygen atoms from the oxalate network. In contrast to **3**, there are hydrogen-bonds between the two crystallographically independent $[Co^{II}(L)_2]^{2+}$ complexes, which involve one NH_2 from triazine and one N atom from the triazine ring of the neighbouring molecule. These interactions lead to isolated chains of hydrogen-bonded $[Co^{II}(L)_2]^{2+}$ complexes running along the *c* axis (see **Fig. S11**). As in oxalate-based compounds based on $[Fe^{II}(L)_2]^{2+}$ and in compound **3**, the structure presents voids filled with disordered solvent molecules. Disordered solvent molecules have been treated with PLATON/SQUEEZE (see experimental section).[5]

Table S1. Crystallographic data for **4**[‡]

Compound	**4**
Empirical formula	$C_{57}H_{37}Co_{1.5}Cr_3Mn_3N_{21}O_{38}$
Formula weight	2033.29
Crystal colour	Pink
Crystal size	0.26*0.22*0.05
Temperature (K)	120(2)
Wavelength (Å)	0.71073
Crystal system, Z	Monoclinic, 4
Space group	$P2_1/n$
a (Å)	27.6225(11)
b (Å)	15.5013(3)
c (Å)	28.2471(12)
β (°)	117.388(5)
V (Å^3)	10739.3(8)
ρ_{calc} (Mg/m^3)	1.258
$\mu(Mo_{K\alpha})$ (mm^{-1})	0.936
2θ range (°)	6.478 to 60.098
Reflns collected	53497
Independent reflns (R_{int})	273692 (0.1209)
L. S. parameters/ restraints	1051/1
$R1(F)$,[a] $I > 2\sigma(I)$	0.1445
$wR2(F^2)$,[b] all data	0.4685
$S(F^2)$,[c] all data	1.049

[a]$R1(F) = \Sigma||F_O|-|F_C||/\Sigma|F_O|$; [b]$wR2(F^2) = [\Sigma w(F_O^2-F_C^2)^2/\Sigma wF_O^4]^{1/2}$; [c]$S(F^2) = [\Sigma w(F_O^2-F_C^2)^2/\Sigma n + r - p)]^{1/2}$

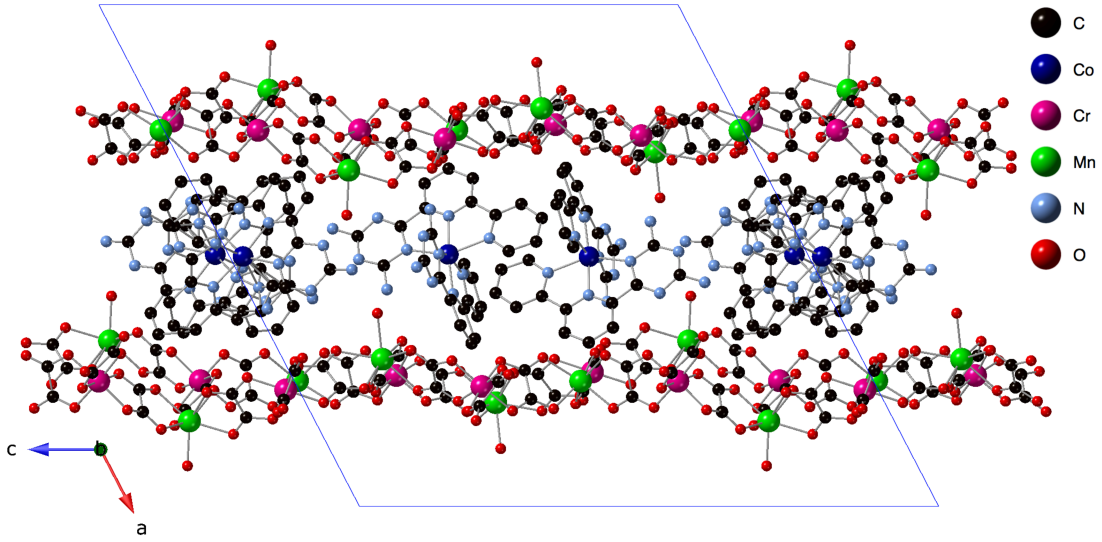

Fig. S10 Projection on the *ac* plane of the structure of **4;** Co (dark blue), Cl (yellow), C (black), N (blue), O (red); hydrogen atoms have been omitted for clarity.

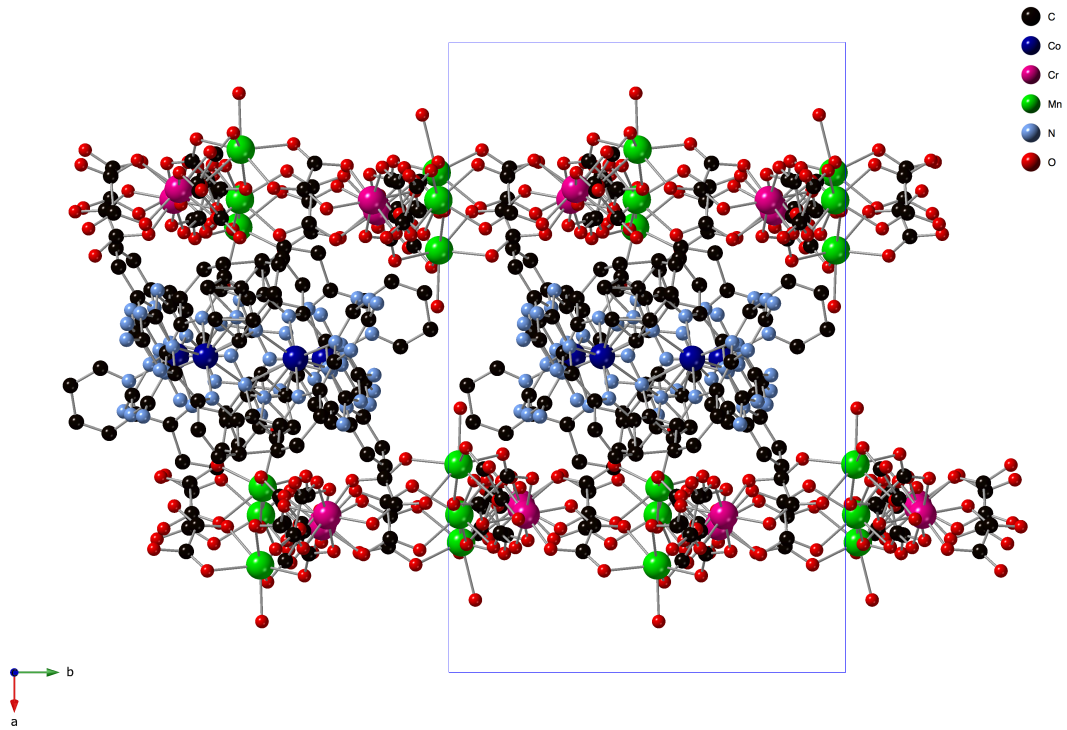

Fig. S11 Projection on the *ab* plane of the structure of **4;** Co (dark blue), Cl (yellow), C (black), N (blue), O (red); hydrogen atoms have been omitted for clarity.

ESI 5. Magnetic properties of 1 and 2

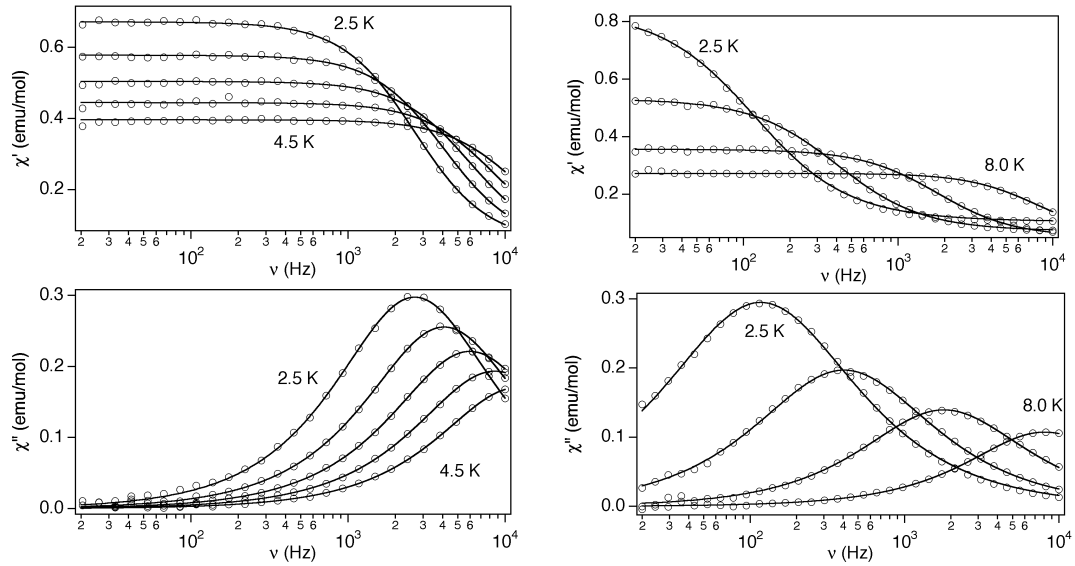

Fig. S12 ac susceptibility in an applied dc field of 0.1 T of **1** (left) and **2** (right) measured as a function of the frequency at the different temperatures (2.5, 3.0, 3.5, 4.0 and 4.5 K for **1**, and 2.5, 4.0, 6.0 and 8.0 K for **2**). Top: Real component. Bottom: Imaginary component. Solid lines represent the best fitting of the experimental data to a Cole-Cole function, yielding R = 0.97-0.98 for **1** and between 0.86-0.98 for **2**.

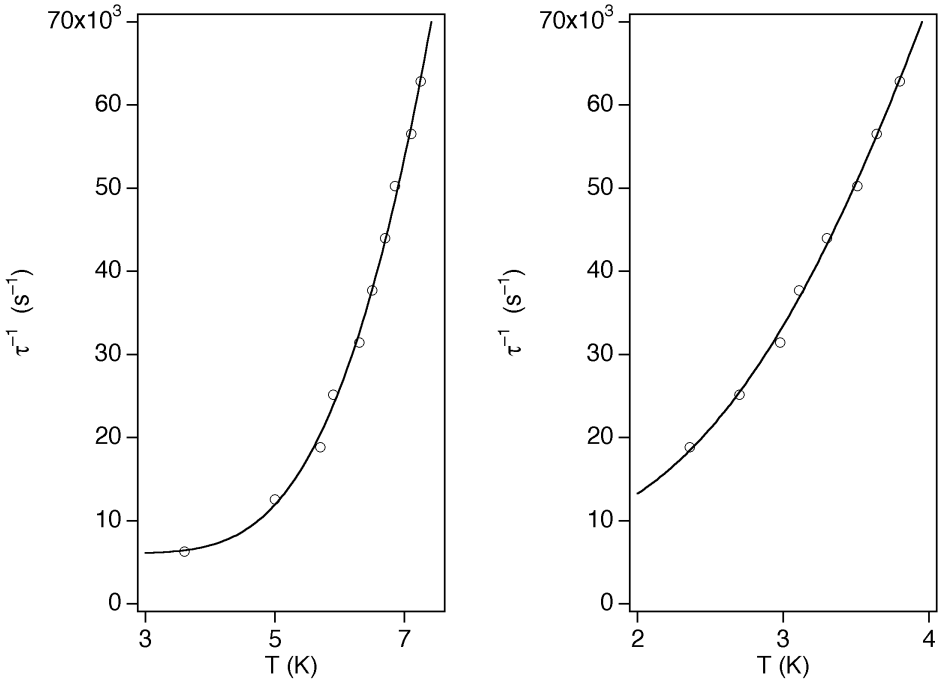

Fig. S13 Thermal dependence of the relaxation time for **1** (left) and **2** (right). Solid lines represent the best fits (see text).

ESI 6. Magnetic properties of 3

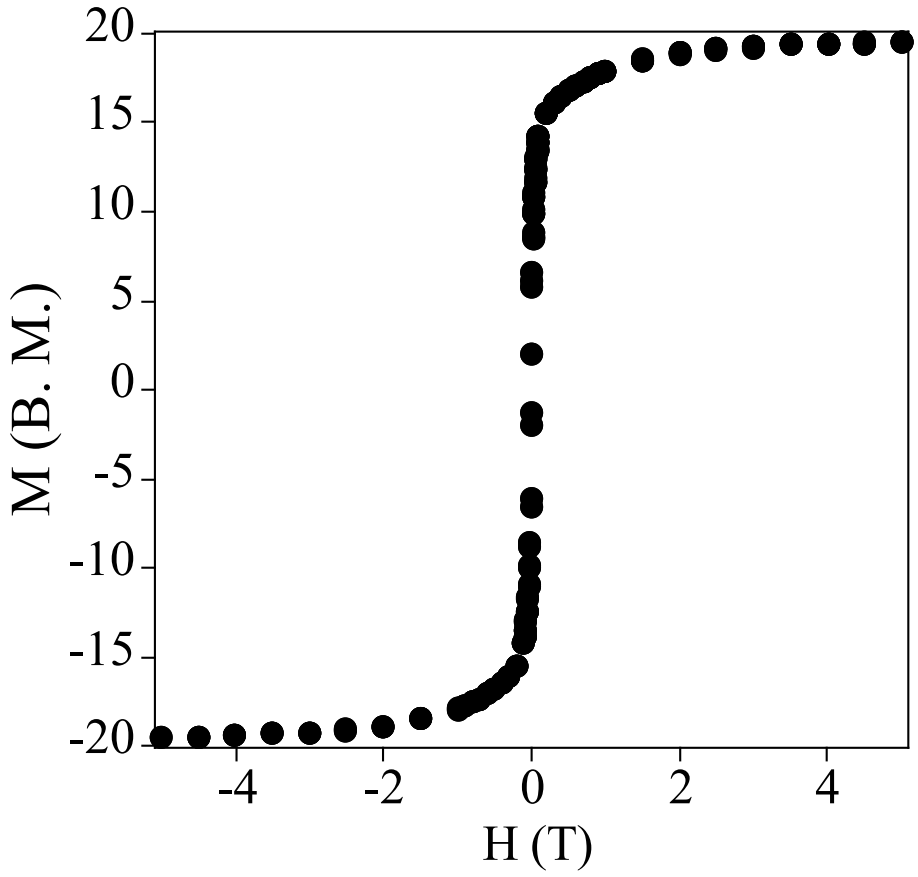

Fig. S14 Magnetization vs magnetic field for **3** measured at T = 2 K.

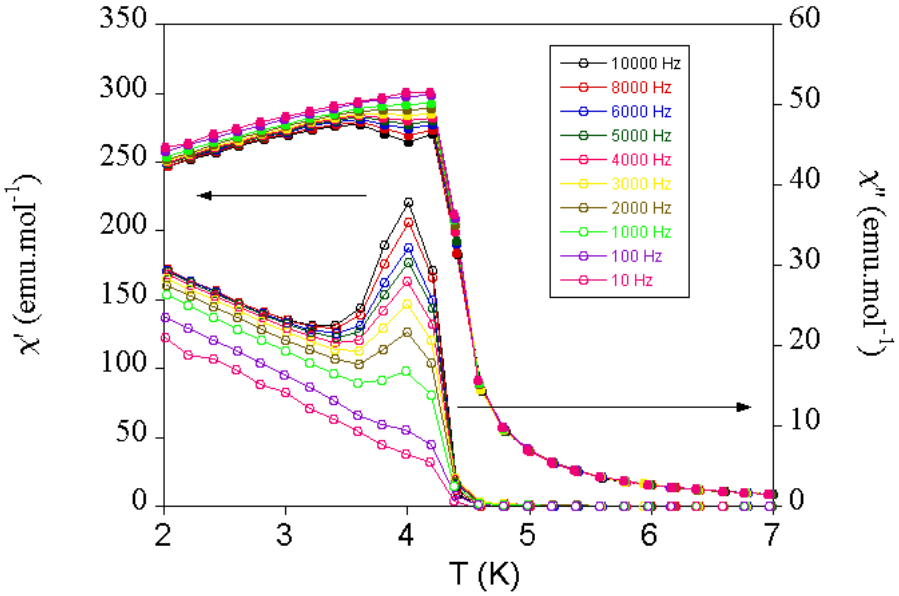
χ' (emu.mol-1)
χ'' (emu.mol-1)
T (K)
10000 Hz
8000 Hz
6000 Hz
5000 Hz
4000 Hz
3000 Hz
2000 Hz
1000 Hz
100 Hz
10 Hz

(a)

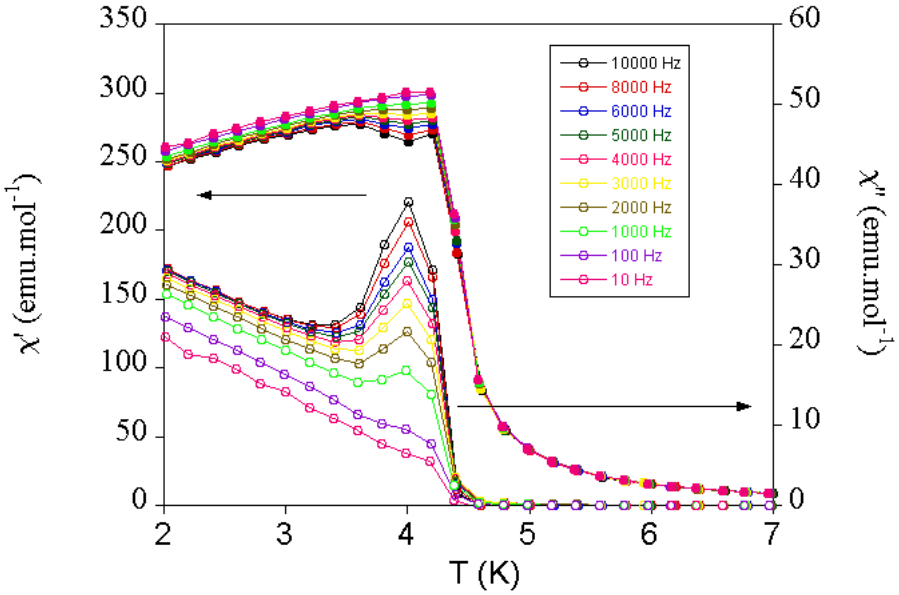
χ' (emu.mol-1)
χ'' (emu.mol-1)
T (K)
10000 Hz
8000 Hz
6000 Hz
5000 Hz
4000 Hz
3000 Hz
2000 Hz
1000 Hz
100 Hz
10 Hz

(b)

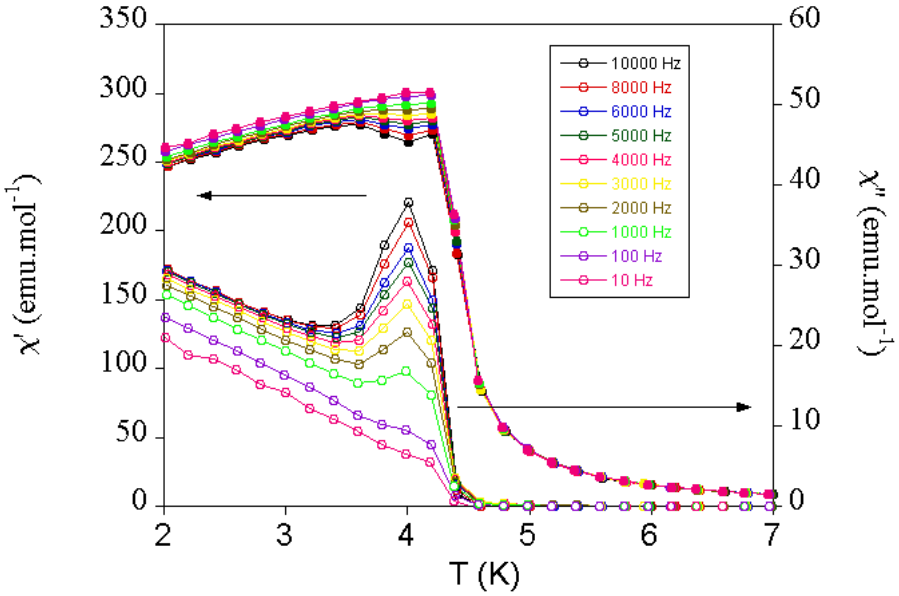

(c)

Fig. S15 Temperature dependence of the in-phase AC susceptibility (χ') (filled symbols) and the out-of-phase AC susceptibility (χ") (empty symbols) for **3** measured at several frequencies and under the action of a dc magnetic field ((a) 0 G, (b) 50 G and (c) 100 G).

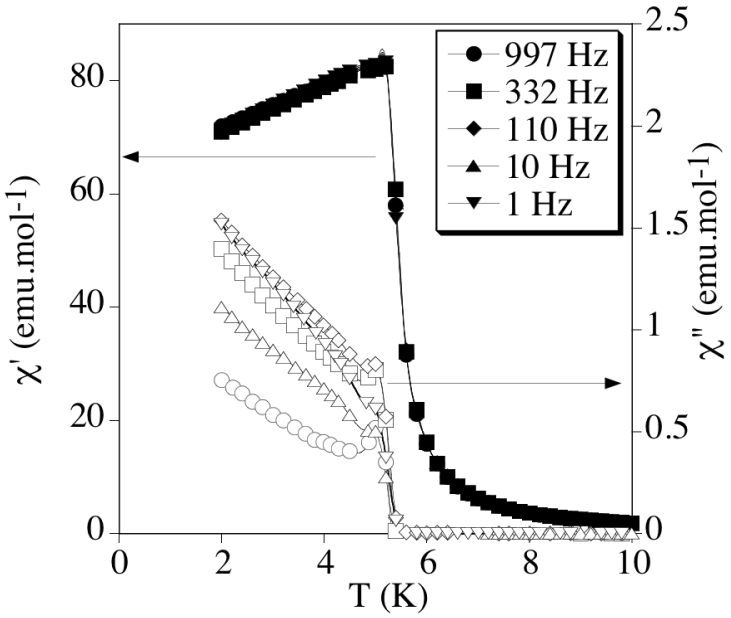
997 Hz
332 Hz
110 Hz
10 Hz
1 Hz
χ' (emu.mol-1)
χ'' (emu.mol-1)
T (K)
0
20
40
60
80
0
0.5
1
1.5
2
2.5
0
2
4
6
8
10

(a)

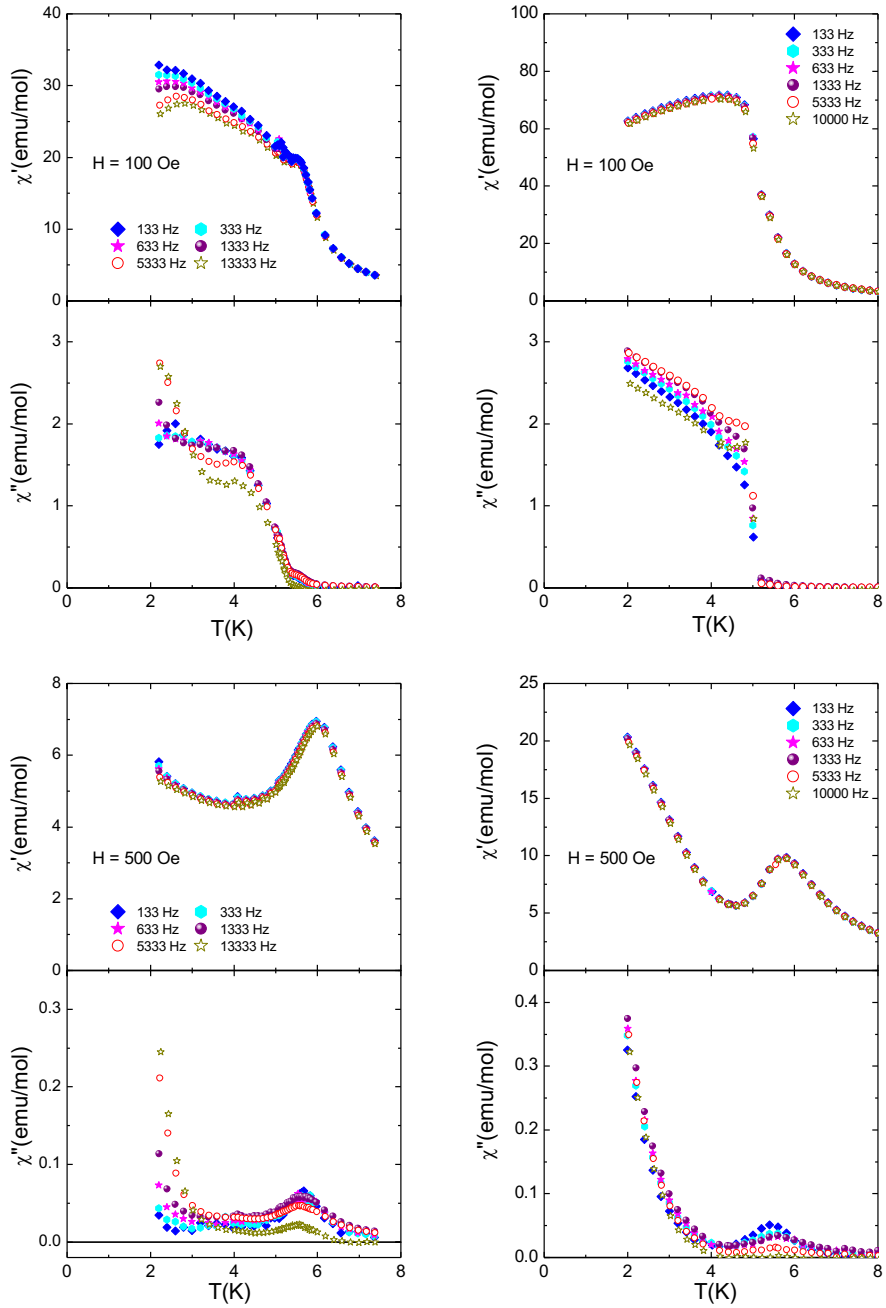

(b)

Fig. S16 AC magnetic susceptibility measurements of [In(sal$_2$-trien)][Mn^{II}Cr^{III}(ox)$_3$]·solv at H = 0 Oe extracted from reference 4b (a). AC magnetic susceptibility of [Mn^{III}(salen)(H$_2$O)]$_2$[Mn^{II}Cr^{III}(ox)$_3$]$_2$·solv measured at H = 100 Oe and 500 Oe and for several frequencies (left), compared with that of [In(sal$_2$-trien)][Mn^{II}Cr^{III}(ox)$_3$]·solv (right) extracted from reference 6 (b).

The thermal dependence of χT of filtered crystals of **3** shows a value of 15.3 $cm^3 \cdot K \cdot mol^{-1}$ at 300 K (see Fig. S17) as that of the sample measured in contact with the mother liquor, which is approximately equal to the sum of the expected contribution for the isolated paramagnetic ions of the oxalate-based network plus the χT of **1** at 300 K (2.7 $cm^3 \cdot K \cdot mol^{-1}$). However, at lower temperatures, χT presents a gradual decrease to reach a minimum value of χT = 13.1 $cm^3 \cdot K \cdot mol^{-1}$ at around 55 K instead of the constant increase observed for the sample measured in contact with the mother liquor. At lower temperature there is a sharp increase of χT indicating the onset of a magnetic ordering. The isothermal *M* of filtered crystals of **3** at 2 K shows a more gradual increase at increasing magnetic fields than that of the solvated sample. In addition to this, it reaches a lower *M* value at 5 T of 13.2 B. M. (19.5 B. M. for the solvated sample) (see Fig. S18). This indicates that *M* of **3** is not a superposition of the magnetization of each of the two components in contrast to the solvated sample. This maximum *M* value is consistent with the expected value for an antiferromagnetic coupling between the magnetic moments of the two subnetworks (16 B. M. for two $Mn^{II}Cr^{III}$ – 2.1 B. M. for Co(II) in **1**) as observed previously in $[Mn^{III}(salen)(H_2O)]_2[Mn^{II}Cr^{III}(ox)_3]_2 \cdot (CH_3OH) \cdot (CH_3CN)_2$.[6] AC susceptibility measurements show a decrease of T_c to a value of 3.2 K in the filtered sample (4.6 K in contact with the mother liquor). Furthermore, it shows a stronger variation with frequency at lower temperatures than that of solvated sample (Fig. S19). All these results could indicate that the magnetic moments of the bimetallic oxalate network and the inserted $[Co^{II}(L)_2]^{2+}$ complexes present some interactions as a consequence of the removal of the solvent molecules of the structure but this has be taken with caution. This drastic change of the magnetic properties after filtering (desolvation) could be also due to changes in distances and angles of the extended bimetallic oxalate-based network. Indeed, PXRD patterns show a complete lack of crystallinity in the filtered sample, which could be a consequence of a collapse of the extended network after removing the solvent molecules.

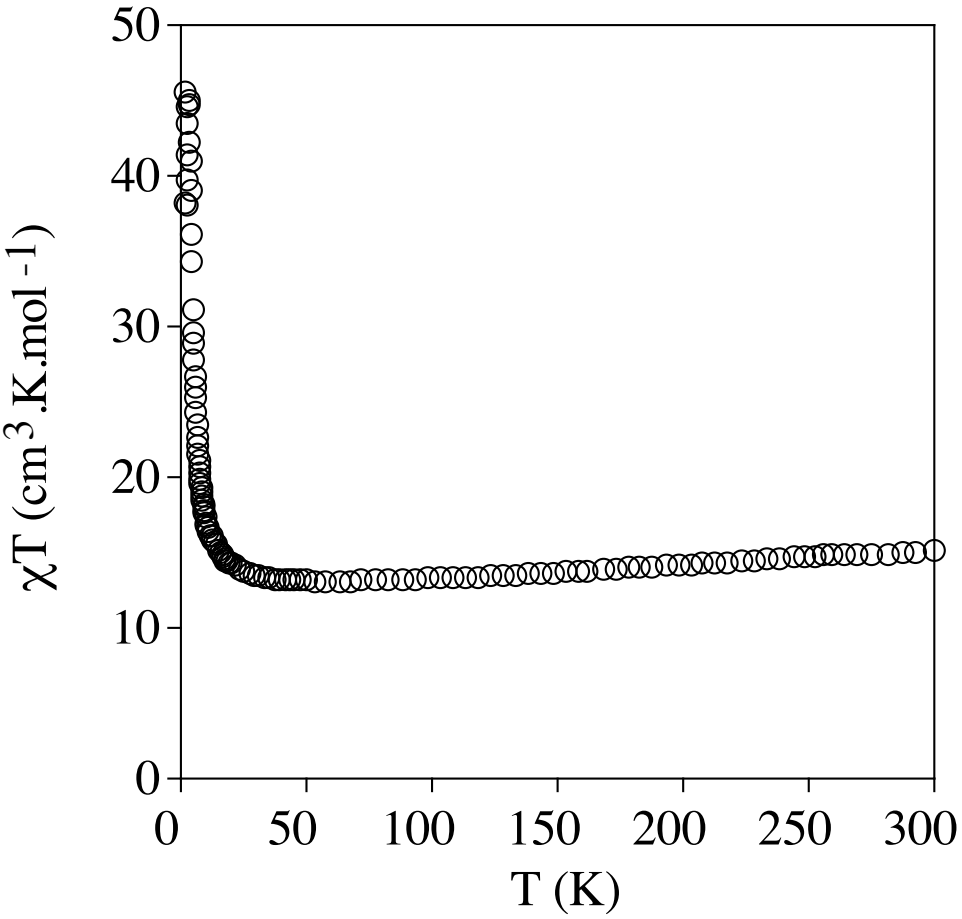

Fig. S17 Temperature dependence of the product of the molar magnetic susceptibility with temperature (χT) at 0.1 T for filtered crystals of **3**.

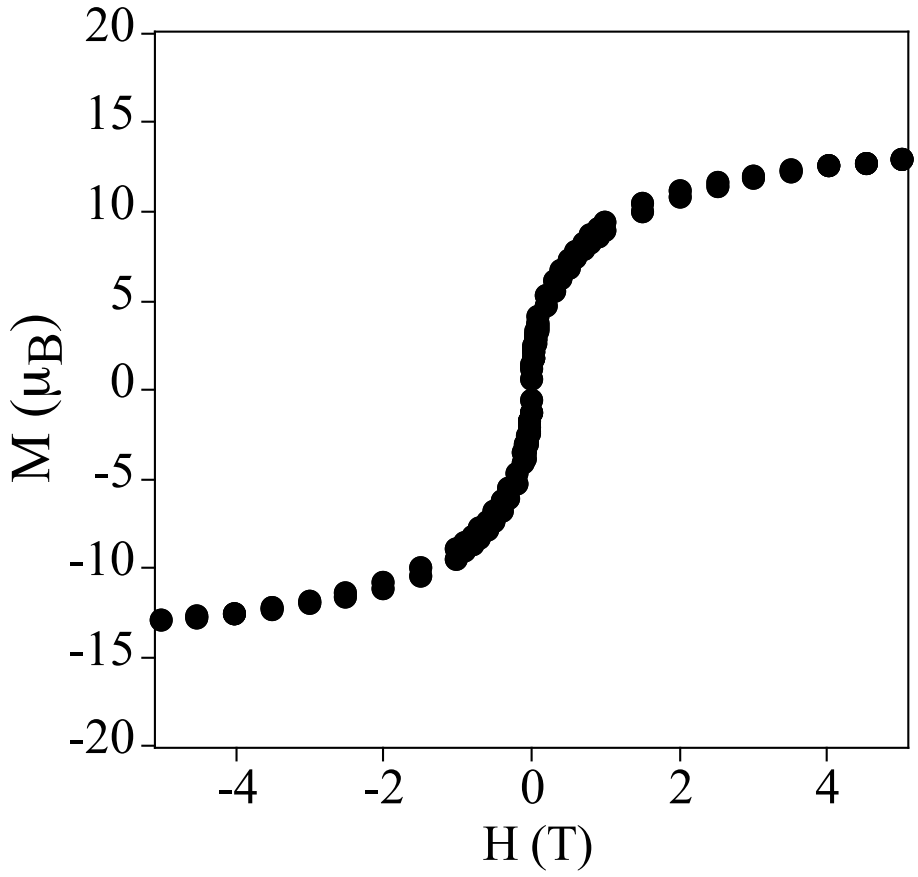

Fig. S18 Field dependence of the magnetization at 2 K for filtered crystals of **3**.

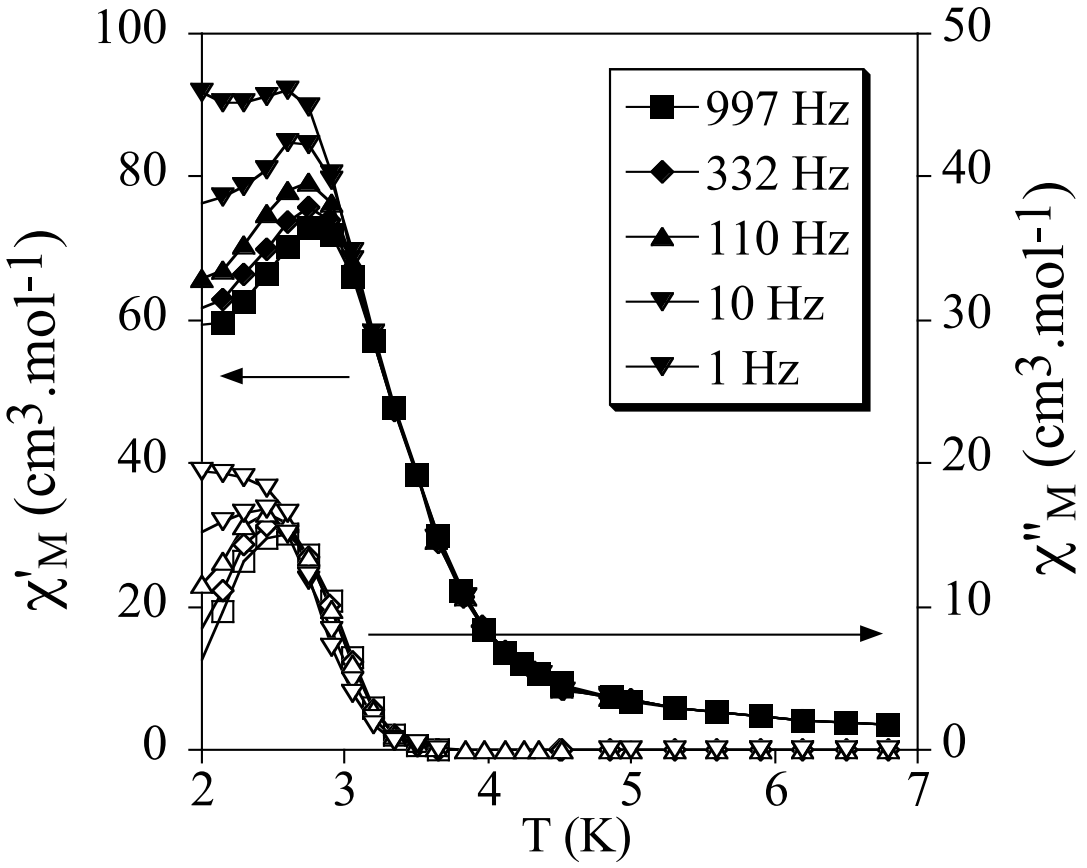

Fig. S19 Temperature dependence of the in-phase AC susceptibility (χ') (filled symbols) and the out-of-phase AC susceptibility (χ'') (empty symbols) for filtered crystals of **3**.

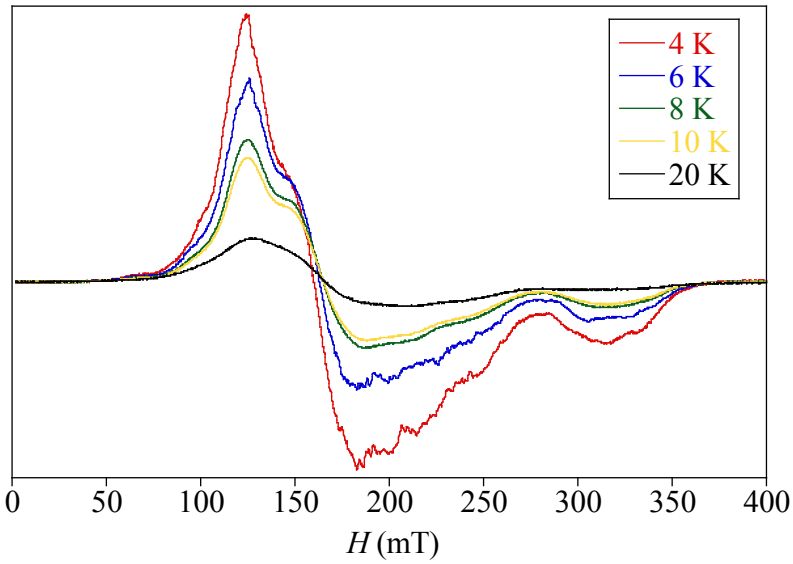

(a)

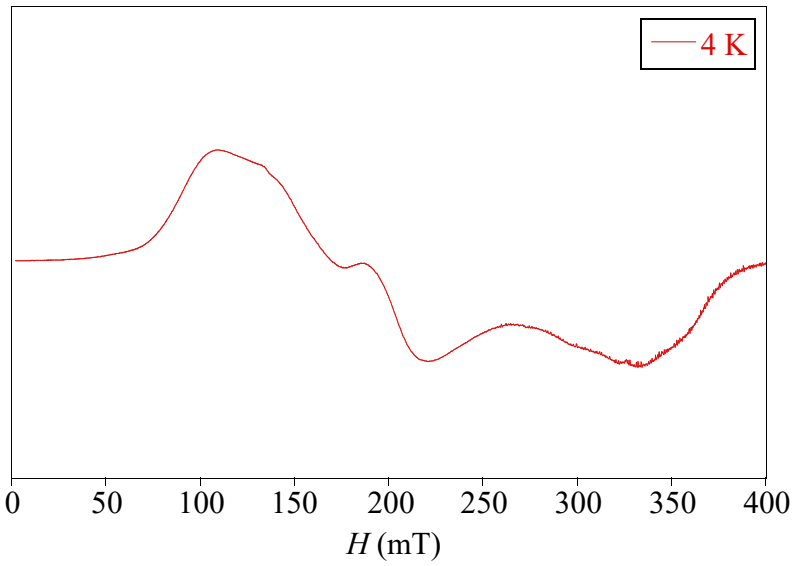

(b)

Fig. S20 EPR spectra of **1** (a) and **2** (b).

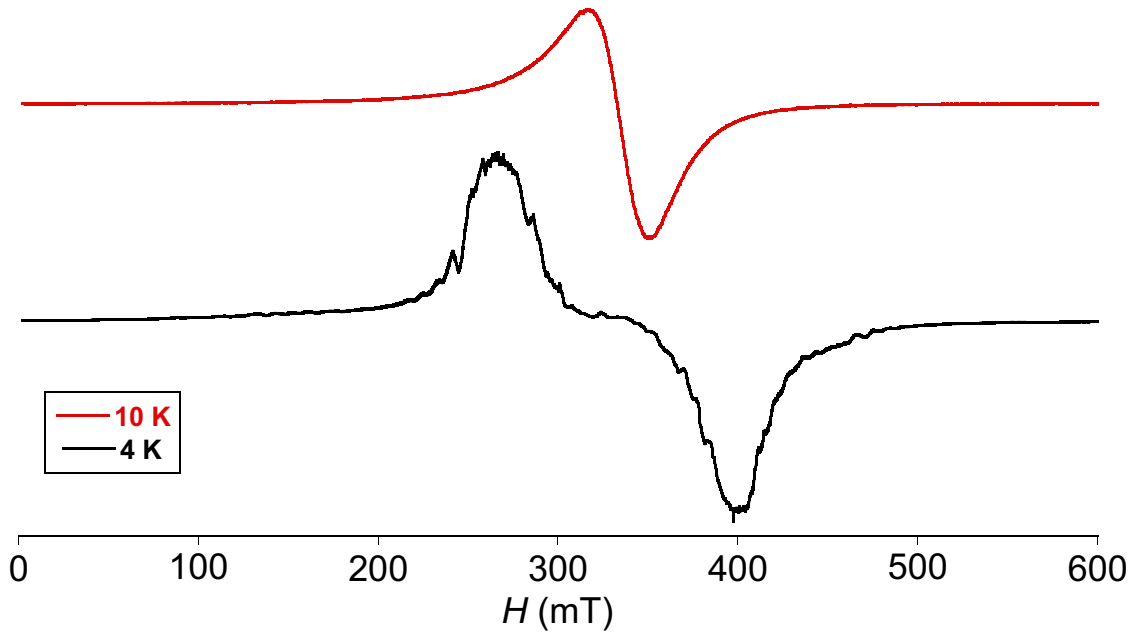

Fig. S21 EPR spectra of **3**.

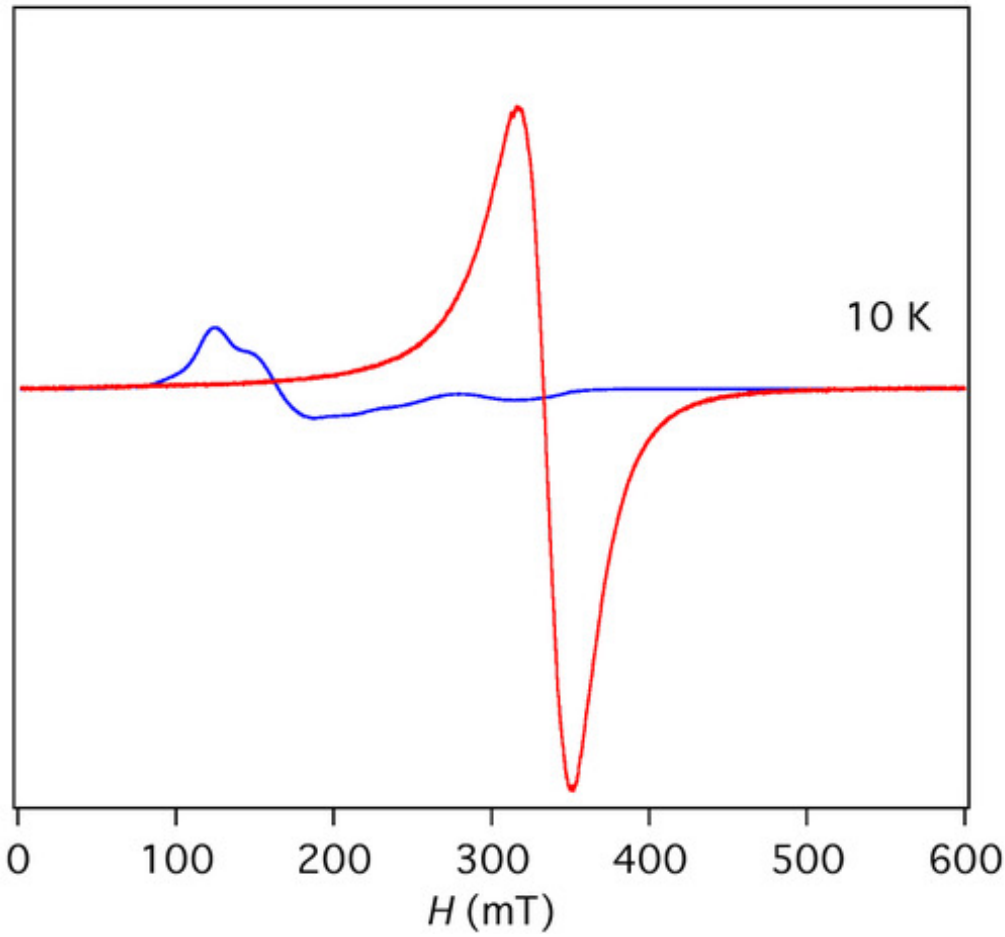

Fig. S22 EPR spectra normalized per mole of **3** (red line) and $[Co^{II}(L)_2]^{2+}$ monomer in **1** (blue line) at 10 K.

1 [1] E. Coronado, J.R. Galán-Mascarós, C. Martí-Gastaldo and A. Murcia-Martínez, *Dalton Trans.*, 2006, **2006**, 3294.

2 [2] M. Clemente-León, E. Coronado, J.C. Dias, A. Soriano-Portillo and R.D. Willett, *Inorg. Chem.*, 2008, **47**, 6458.

3 [3] C. Sánchez-Sánchez, C. Desplanches, J. M. Clemente-Juan, M. Clemente-León and E. Coronado, *Dalton Trans.,* 2017, **46**, 2680.

4 [4]*(a)* M. Clemente-León, E. Coronado, M. C. Giménez-López, A. Soriano-Portillo, J. C. Waerenborgh, F. S. Delgado and C. Ruiz-Pérez, *Inorg. Chem.*, 2008, **47**, 9111; *(b)* M. Clemente-León, E. Coronado, M. López-Jordà, G. Mínguez Espallargas, A. Soriano-Portillo and J. C. Waerenborgh, *Chem. Eur., J.*, 2010, **16**, 2207; *(c)* M. Clemente-León, E. Coronado and M. López-Jordà, *Dalton Trans.*, 2010, **39**, 4903; *(d)* M. Clemente-León, E. Coronado, M. López-Jordà and J. C. Waerenborgh, *Inorg. Chem.*, 2011, **50**, 9122; *(e)* M. Clemente-León, E. Coronado, M. López-Jordà, C. Desplanches, S. Asthana, H. Wang and J.-F. Létard, *Chem. Sci.,* 2011, **2**, 1121; *(f)* M. Clemente-León, E. Coronado and M. López-Jordà, *Eur. J. Inorg. Chem.,* 2013, 753; *(g)* M. Clemente-León, E. Coronado, M. López-Jordà, J. C. Waerenborgh, C. Desplanches, H. Wang, J.-F. Létard, A. Hauser and A. Tissot, *J. Am. Chem.* Soc., 2013, **135**, 8655.

5 [5] J. Spek, *Appl. Cryst.,* 2003, **36**, 7.

6 [6]M. Clemente-León, E. Coronado, C. J. Gómez-García, M. López-Jordà, A. Camón, A. Repollés and F. Luis, *Chem. Eur. J.*, 2014, **20**, 1669.